Design of Bipolar MT HVDC Grids: Contingency Analysis and Preliminary Dynamic Studies

C. Cardozo, H. Clémot, B. De Foucaud, J. Pouget, P. Rault, S. Dennetière, T. Qoria, S. Hansen.

***Abstract*—This paper presents a scenario-based approach for steady-state design studies of Multi-Terminal HVDC grids, focusing on a pole-wise and multi-slope droop control strategy. Two configurations are analyzed, with and without offshore wind generation, while taking into account the presence of DC circuit breakers. Using DC load flow calculations and contingency analysis, DC voltage secure operating ranges and preliminary droop gains are determined to ensure compliance with the N-1 rule, maintaining post-contingency DC voltage within the continuous operating range. The impact of neutral voltage shifts during asymmetrical operation on pole-to-ground voltages, as well as the challenges of designing primary DC voltage control in highly inductive DC grids are also highlighted. The approach is validated with dynamic simulations.**

***Keywords*—Multi-terminal HVDC, bipole, offshore wind farm, multi-slope DC voltage droop control.**

I. Introduction

DRIVEN by the ever-increasing size of Offshore Wind Farm (OWF) installations and the growing rating of cross-country interconnections, bipolar Modular Multilevel Converter (MMC)-based High Voltage Direct Current (HVDC) solutions are anticipated to play an important role in future transmission networks, with 450 GW of offshore wind by 2050 planned in Europe. At the same time, concerns about the techno-economic feasibility of developing such projects in a point-to-point setting have prompted the industry to address the challenges associated with transitioning to a Multi-Terminal (MT) configuration.

The development of suitable technical specifications, operational strategies, and control solutions to mitigate the unique risks inherent to these complex systems has been widely explored over the past decade [1], [2]. Research spans various areas, including DC Load Flow (LF) [3] and dynamic performance analyses with a focus on distributed DC voltage control, stability properties [4], as well as DC fault handling [5], [6]. More recently, significant attention has been given to the impact of system topology, particularly the bipolar configuration [7], [8], and to interoperability challenges introduced by a multi-vendor framework [9].

Co-funded by the European Union. Views and opinions expressed are, however, those of the author(s) only and do not necessarily reflect those of the European Union or CINEA. Neither the European Union nor the granting authority can be held responsible for them. Grant agreement: 101095874.
C. Cardozo, H. Clémot, B. De Foucaud, J. Pouget, P. Rault and S. Dennetière are with RTE, 7C, place du Dôme 92073 Paris La Defense, France (e-mail of corresponding author: carmen.cardozo@rte-france.com). T. Qoria is with GE Vernova - Grid Solutions, Culemeyerstr. 1 I 12277 Berlin, Germany. S. Hansen is with Hitachi Energy - HVDC, Lyviksvägen 3, 771 80, Ludvika, Sweden.
Paper submitted to the International Conference on Power Systems Transients (IPST2025) in Guadalajara, Mexico, June 8-12, 2025.

In this context, the InterOPERA project was launched to enable future HVDC systems from different suppliers to operate together. This initiative paves the way for the first real-life MT, multi-vendor, multi-purpose HVDC projects in Europe. The project has already delivered significant contributions, including the development of common functional specifications [10] and minimum requirements for interfaces [11]. Beyond advancing technical standards, InterOPERA will also provide guidelines on procurement, commercial practices, and legal and regulatory frameworks to streamline tendering processes [12]. Finally, a Real-Time (RT) demonstrator will be implemented to validate and refine the proposed methods and processes, ensuring practical applicability. This work focuses on activities supporting the deployment of the RT demonstrator, particularly HVDC grid design studies conducted using generic models. Specifically, three study packages have been defined:

- Steady-state studies supported by DC LF-based contingency analyses to ensure that considered DC voltage regulation capabilities and continuous operating ranges align with system operation under the selected risk policy, typically the N-1 criterion.
- Dynamic studies to verify system's proper behavior during contingencies, ensuring that temporary excursions of electrical quantities remain within equipment capabilities, preventing undesirable protection operations.
- Transient studies to assess the required withstand capabilities of network assets and grid-connected devices in light of the performance of available protection systems, while ensuring proper insulation coordination.

This paper focuses on contingency analyses based on DC LF calculations and dynamic simulations, with ongoing work dedicated to DC fault and transient studies. The main contribution lies in the proposed methodology for conducting pre-tender planning studies for MT multi-vendor projects, in which additional technical specifications must be defined at the DC point of connection. The approach is applied to the InterOPERA demonstrator's topology to support the detailed specification of various subsystems.

This paper is organized as follows: Section II outlines the overall methodological approach and describes the system under study. Section III presents LF calculations for the N situations, providing valid initial Operating Conditions (OCs) for the contingency analysis. Section IV discusses key findings regarding the final states following the action of the primary DC voltage control, while Section V focuses on its dynamic performance. Finally, conclusions are presented in Section VI.

II. Methodology and Modeling Overview

Sections II-A to II-C outline the methodology, including guidelines for defining relevant scenarios and preliminary operational settings for the contingency analysis. Sections II-D to II-E then describe the considered Three-Terminal (3T) system and the simulation methods employed.

A. Defining Scenarios for the Contingency Analysis

The DC LF study primarily focuses on steady-state currents and voltage drops across the MT HVDC grid, evaluating various OCs that typically involve maximum power transfer and extreme voltage values at each AC/DC converter station. Design scenarios can be defined based on the lower DC voltage limit for continuous operation, resulting in maximum current and, consequently, the largest anticipated voltage drops. However, these scenarios are unsuitable for defining realistic initial OCs for contingency analysis, as they would lead to security violations following single outages.

1) Valid Initial OCs: in practice, they are expected to be defined by an upper-level controller [13], [14]. Typically, a DC grid controller adjusts DC voltage and active power references while pursuing various operational objectives. To simplify design studies and eliminate the need to implement the underlying algorithms, voltage and active power references for each onshore station operating in DC voltage droop mode ($U_{DC,0}$, $P_{DC,0}$) can be determined through LF calculations of carefully selected scenarios. Specifically, valid initial OCs, referred to as *N situations*, are established by defining a *secure operating range* and setting the AC/DC converter station voltages at its boundaries. Ensuring the existence of this range, while aligning with practical primary DC voltage control settings, is a key outcome of the design studies.

2) The Contingency List: in line with the European System Operation Guideline (SOGL) [15], two types of contingency scenarios can be defined for design purposes:

- *Ordinary contingency*, involving the single outage of any individual asset.
- *Exceptional contingency*, involving simultaneous outages with a common cause.

The use of bundled cables or coupled busbar topologies exposes the system to common failure modes, making the loss of an entire bipole an exceptional contingency. Consequently, this scenario will be examined in this study, alongside single outages. By definition, *out-of-range contingencies* are beyond the scope of this work.

B. DC LF-based Contingency Analysis

Starting from a *preliminary* secure operating range and primary DC voltage control settings, the final states after its action are computed for each outage in the contingency list and for each predefined N situation [16]. If the final system state violates the Operational Security Limits (OSL), defined here as the continuous operating range for DC power, voltage, and current, adjustments are made to operational parameters—such as refining primary DC voltage control settings or, if necessary, modifying the secure operating range—before considering hardware upgrades; namely, expanding OSL.

C. Preliminary Settings for the Contingency Analysis

Following the recommendations from [10], inspired by capability requirements for primary frequency control applied to AC system-connected devices, two types of DC Voltage Sensitive Modes (DCVSM) are considered. Both employ the classical droop equation (1), but operate within a specific band with dedicated settings (s_i) as illustrated in Fig. 1:

$$P_{DC} = P_{DC,0} + \frac{1}{s_i}(U_{DC,0} - U_{DC}) \tag{1}$$

- DCVSM operates under normal conditions to ensure continuous power balance and DC voltage regulation while distributing the control effort across units.
- Limited DCVSM (LDCVSM) provides stronger DC voltage support when the DC voltage approaches the system OSL, typically during severe disturbances that lead to large power imbalances.

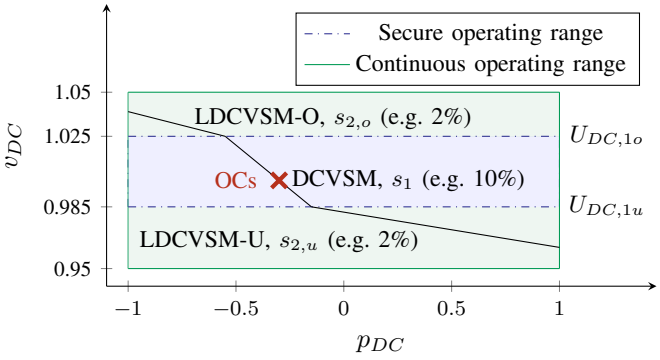

Fig. 1. Continuous and secure operating ranges in the p_{DC}-v_{DC} plane

LDCVSM is divided into two types based on the direction of voltage deviation: LDCVSM-O/U (for over/undervoltage), allowing for differentiated slopes to accommodate asymmetrical system needs and asset capabilities. Thresholds for limited modes ($U_{DC,1u}$ and $U_{DC,1o}$) are set at the boundaries of the secure operating range, with the knee points at these limits.

D. System under study

Fig. 2 depicts the test system. Key design premises include:

- AC/DC converter stations are based on a bipolar topology, rated at 2 GW (1 GW per pole).
- The continuous operating range is defined as ±5% of the nominal DC grid voltage ($U_{DC,Nom}$), set to 500 kV. Therefore, the system's maximum continuous operating voltage is 525 kV (1.05 pu, with $U_{DC,Base} = U_{DC,Nom}$).
- The system must remain within the continuous operating range for predefined contingencies, relying exclusively on local primary DC voltage control actions.
- Only onshore stations contribute to DC voltage control by implementing a pole-wise droop-type DC voltage controller. No local balancing strategy is considered.
- DC voltage control is based on pole-to-neutral quantities.
- Offshore stations, feeding full OWF generation, are modeled as constant power sources.

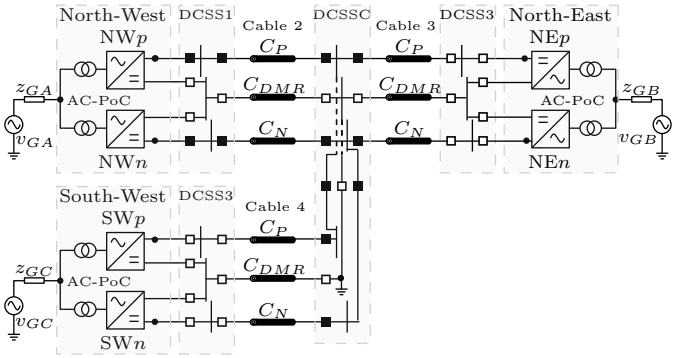

Fig. 2. Test system: 3T topology

- A certain degree of selectivity is assumed necessary, requiring the installation of DC circuit breakers.
- A single cable dataset from [17] is used, without distinguishing underground from undersea sections.
- Two configurations are considered: GGG, with all three AC/DC converter stations connected to different onshore grids; and GGW, with one station, North-East (NE), connected to an OWF and operating in Vf mode.

An initial secure operating range is proposed at [492.5, 512.5] kV ([0.985, 1.025] pu) and it is applied to all AC/DC converter stations, with the following preliminary settings for primary DC voltage control:

- DCVSM droop gain (s_1) is set to 10%, and
- LDCVSM droop gain ($s_{2,u} = s_{2,o}$) is set to 2%.

In practice, the secure operating range may include active power restrictions to ensure reserve availability. Current limits may constraint active power at low voltages. However, in the 3T case under study, sufficient capacity is naturally available. Consequently, this consideration is excluded without loss of generality, with the analysis focusing on other aspects.

E. Dynamic Simulations

EMTP® is used to perform Time-Domain (TD) simulations, with test system modeling details provided in Appendix VII. Main simulation settings include the integration method (Trapezoidal and Backward Euler), with a time step of 20 μs. Outages are simulated by the forced blocking (triggered by an external signal) of one (or both) AC/DC poles while remaining connected. The other units will continue normal operation. Events are applied at 2 s to allow for the initialization phase, and the total simulation duration is set to 3 s, as the dynamic phenomena of interest are expected to vanish within 1 s.

III. DC Load Flow Calculations in N

Tables I and II lists the twelve initial OCs (N situations) considered in this study for the 3T-GGG configuration. Only a subset of these applies to configurations involving OWF, as OWF-connected converters always operate in rectifier mode. In **bold** are the imposed quantities that define the scenario, and in *italic* are the results of the LF calculation. Active power is considered positive when injected into the DC grid. Both single pole and bipole outages of each station are considered, resulting in six potential contingencies.

TABLE I
N SITUATIONS - LOW VOLTAGE CASES (PU)

OCs	N1a	N1b	N2a	N2b	N3a	N3b
U_{NW} (pu)	**0.985**	**0.985**	*1.017*	*1.002*	*1.006*	*0.991*
P_{NW} (pu)	**-1**	**-1**	**1**	*0.022*	**1**	*0.022*
U_{SW} (pu)	*1.017*	*1.001*	**0.985**	**0.985**	*0.991*	*1.007*
P_{SW} (pu)	**1**	*0.021*	**-1**	**-1**	*0.021*	**1**
U_{NE} (pu)	*1.001*	*1.006*	*1.002*	*1.007*	**0.985**	**0.985**
P_{NE} (pu)	*0.032*	**1**	*0.032*	**1**	**-1**	**-1**

TABLE II
N SITUATIONS - HIGH VOLTAGE CASES (PU)

OCs	N4a	N4b	N5a	N5b	N6a	N6b
U_{NW} (pu)	**1.025**	**1.025**	*0.993*	*1.009*	*1.005*	*1.020*
P_{NW} (pu)	**1**	**1**	**-1**	*0.021*	**-1**	*0.021*
U_{SW} (pu)	*0.993*	*1.010*	**1.025**	**1.025**	*1.020*	*1.003*
P_{SW} (pu)	**-1**	*0.020*	**1**	**1**	*0.020*	**-1**
U_{NE} (pu)	*1.010*	*1.005*	*1.009*	*1.004*	**1.025**	**1.025**
P_{NE} (pu)	*0.032*	**-1**	*0.032*	**-1**	**1**	**1**

Consequently, a total of 72 (12x6) and 48 (8x6) scenarios are analyzed for the GGG and GGW configurations, respectively. Symmetry within the test system topology can be leveraged to reduce the number of initial OCs evaluations and eliminate some N-1 scenarios. For instance, identical cables #2 and #4, along with consistent station types for NW and SW across all configurations, render scenarios 1 and 2 equivalent.

Fig. 3 shows the DC LF results for N1a and N5a situations, demonstrating that the proposed secure operating range accommodates voltage drops across the MT HVDC grid, with the available regulating margins for primary DC voltage control clearly visualized. The remaining scenarios are omitted for brevity and will be revisited in the contingency analysis, where the LF results in N establish the initial OCs.

Notably, for the LF investigations, a relatively high resistance value (285 mΩ) for the Fault Separation Device (FSD) is assumed and applied to all DC Switching Station (DCSS) stations to ensure conservative results. This assumption will be refined in subsequent TD studies.

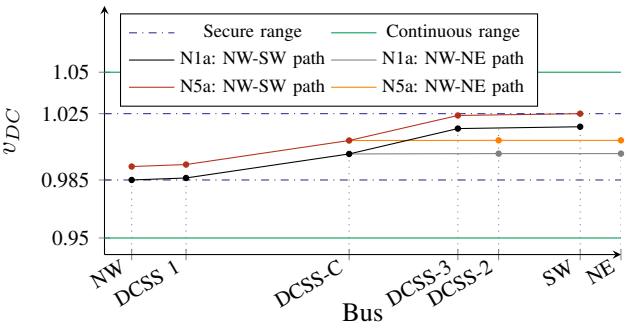

Fig. 3. Voltage profile across the DC grid in N1a and N5a situations

IV. Contingency Analysis

Table III presents LF calculations following the outage of the NW negative pole (asymmetrical), considering the proposed primary DC voltage control settings (10% in DCVSM and 2% in LDCVSM). DC power and pole-to-neutral voltage are in pu, with 1000 MW and 500 kV as bases.

TABLE III
LOAD FLOW RESULTS FOR N1A FOLLOWING NWN OUTAGE (PU)

Pole	U_{NW}	P_{NW}	U_{SW}	P_{SW}	U_{NE}	P_{NE}
Positive	0.982	-0.842	1.025	0.899	1.006	-0.02
Negative	-1.043	0	-1.035	0.447	-1.030	-0.445

Fig. 4 shows this results in the p_{DC}-v_{DC} plane, where:

- The red cross (x) indicates the initial operating point of each terminal for the selected N situation (N1a).
- The orange circle (o) represents the final operating point of the healthy pole (positive in this case).
- The orange plus (+) indicates the final operating point of the affected pole (negative in this case).

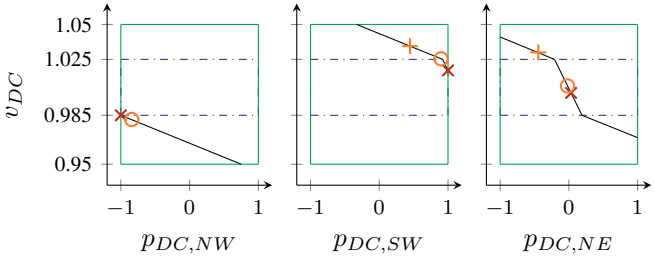

Fig. 4. DC voltage control response: N1a, outage of the NW negative pole (asymmetrical contingency). NW (left), SW (middle) NE (right)

On the affected (negative) pole, both surviving stations (SW and NE) share the control effort according to their identical droop settings, though the grid topology also influences this distribution. As a result, the power transfer is reduced to approximately 0.45 pu (450 MW), which is now exported to NE. However, the asymmetrical operation results in current flow through the Dedicated Metallic Return (DMR). This shift in current from the negative pole to the DMR is perceived by the NW healthy (positive) pole as an increase in effective resistance, resulting in a load flow change and, consequently, a regulation error. The active power flow between NW and SW is slightly reduced. At NE positive pole, the flow is reversed while remaining relatively low. With the grounding point considered at the central DCSS, deviations in the neutral voltages of all AC/DC stations occur.

A. Results for the GGG configuration

Fig. 5 presents results for all scenarios under relevant contingencies. For clarity, the outage of the idling station is excluded, with a focus on outages at stations operating at full power. As before:

- Crosses (x) represent the initial OCs
- Circles (o) indicate the final state of the healthy (positive) pole after the negative pole outage at the affected station
- Pluses (+) mark the affected (negative) pole on the surviving stations
- Squares are used to indicate the healthy pole on the surviving stations (the outage is in another station)
- Diamonds represent bipole outage results.

Different colors represent various N situations. It is observed that in all cases, DC voltages remain within the OSL.

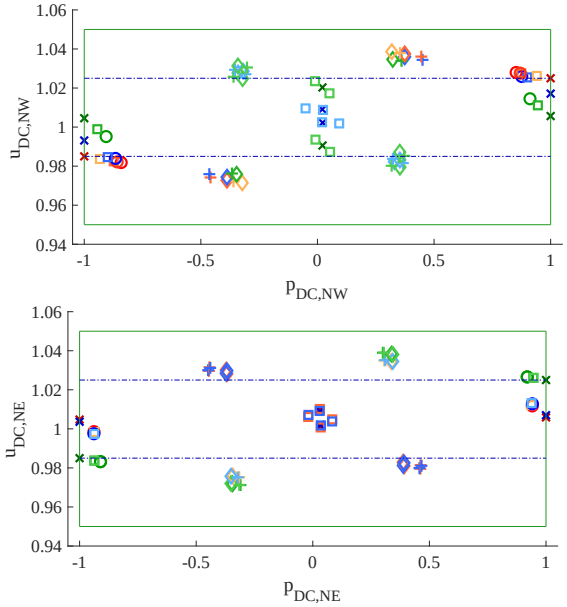

Fig. 5. GGG configuration: contingency analysis. NW (top), NE (bottom)

SW results are similar to NW due to the system symmetry and are excluded for brevity. Although the proposed secure operating range and primary DC voltage control settings for the GGG configuration effectively meet the design criteria when focusing on pole-to-neutral quantities, attention must be given to the pole-to-ground DC voltages. Due to asymmetrical operation, neutral voltages reach 5.18 kV (0.0104 pu) at NW, -2.69 kV (0.0054 pu) at SW, and -0.36 kV (0.0007 pu) at NE.

Fig. 6 illustrates the pole-to-ground DC voltage at the three converter stations by adding neutral voltages to the pole-to-neutral values already presented in Fig. 4 (outage of the negative pole at NW, starting from situation N1a).

The voltage at the NW positive pole, measured to ground, rises from 0.982 pu to 0.992 pu (490.92 kV to 496.1 kV). In contrast, the SW positive pole voltage decreases to 1.02 pu (from 512.7 kV to 510 kV). For the negative pole, the shift occurs in the opposite direction (in terms of magnitude), with the pole-to-ground DC voltage at the SW negative pole reaching -1.04 pu (from -517.24 kV to -519.93 kV).

On the blocked pole (labeled *Outage*), the pole-to-ground DC voltage matches the negative pole DC voltage at the central DCSS (-1.033 pu, -516.33 kV), the pole-to-neutral DC voltage then reaches -1.043 pu (-521.51 kV).

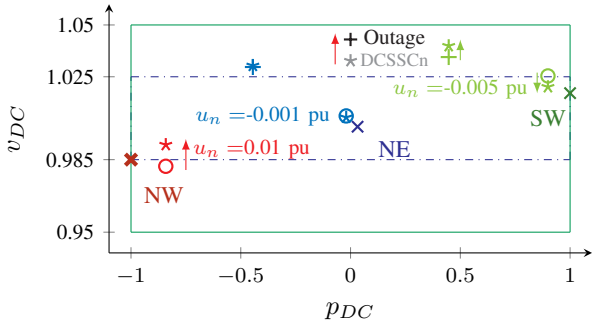

Fig. 6. Pole-to-ground DC voltage: N1a, outage of the NW negative pole

B. GGW configuration: OWF at NE station

Fig. 7 shows LF results for three outages initialized at N1b:

- NW negative pole outage (orange o and +)
- NW bipole outage (◇)
- NE negative pole outage (purple △ for the healthy, positive, pole; pink □ for the affected, negative, pole)

In the GGW configuration, the proposed secure range fails to maintain operational security in the most critical, recognized extreme, scenario: when OWF is exporting maximum generation to the affected station, and the surviving onshore station must fully compensate for the entire initial power transfer. In this case, the DC voltage at the affected pole of the NE station reaches 531.5 kV (1.063 pu), even after reducing the LDCVSM gain to 1% in the onshore stations.

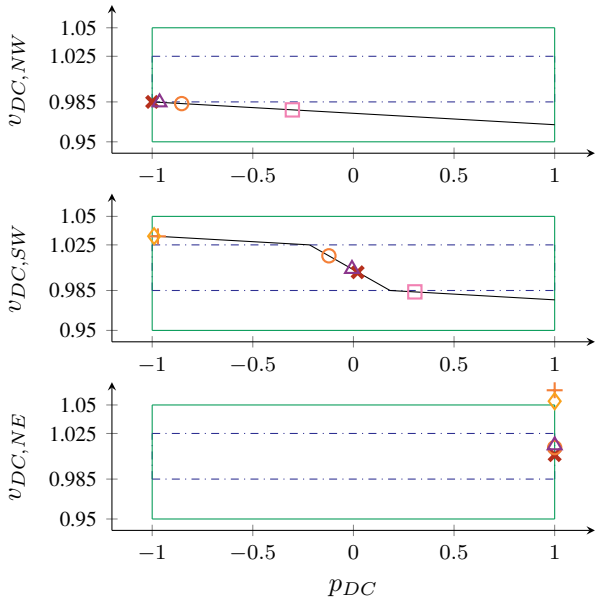

Fig. 7. GGW: primary DC voltage control response for N1b, NW & NE single pole outage, NW bipole outage. NW (top), SW (middle), NE (bottom)

As illustrated in Fig. 8, to meet the selected risk policy without a design upgrade, the secure operating range must be shifted downward. After several iterations, the upper bound, $U_{DC,1o}$, is set to 505 kV (1.01 pu on a 500 kV base). Initially, the lower bound, $U_{DC,1u}$ was set to 485 kV (0.97 pu on a 500 kV base) to maintain a 4% range (the width of the blue box). However, violations of the OSL in low-voltage scenarios led to an adjustment to 487.5 kV (0.975 pu on a 500 kV base), revealing an extremely narrow available design space.

C. Discussion on Remedial Actions

In the GGW configuration, the maximum secure operating voltage was limited to 1.01 pu (505 kV), imposing significant operational constraints and increasing system losses. Although excluded from the InterOPERA project, an alternative approach could involve allowing brief overvoltage periods to enable secondary control and centralized redispatch actions, including fast wind power curtailment. Remedial actions and *abnormal* operating ranges, along with permissible durations, for each subsystem must then be specified.

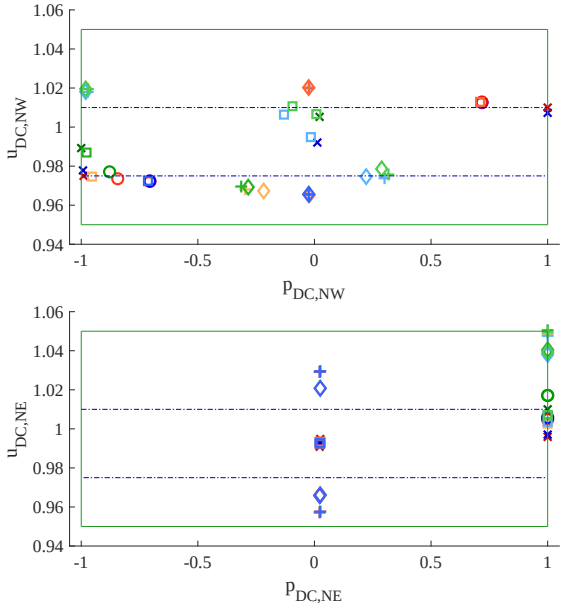

Fig. 8. GGW configuration: Contingency analysis. NW (top), NE (bottom)

V. Preliminary Dynamic Studies

The DC LF-based contingency analysis has been validated with detailed dynamic representation of subsystems using the simulation tool EMTP® (see Appendix VII). The FSD are now modeled by 200 mH reactors at specific locations, which significantly increase DC grid inductance, challenging voltage control and making the system prone to resonance phenomena as illustrated in Section V-A. Section V-B examines the primary DC voltage control step response, while Section V-C discusses system behavior under larger disturbances. Lastly, Section V-D presents final states after the primary DC voltage control action. All 120 scenarios were simulated in under one hour on a standard personal workstation (11th Gen Inter(R) Core (TM) i7-11850H @2.50 GHz).

A. DC Grid Frequency Scan

Fig. 9 shows the DC grid frequency scan at each DC point of connection (only grid, no converters), limited to 500 Hz for readability purposes. A slight resonance near 30 Hz is observed when connecting to NW and SW, becoming excited in the blocking case (see Fig. 11). Additionally, a pronounced peak around 85 Hz is identified at the NE DC point of connection. At NW, the DC grid exhibits an inductive behavior, characterized by a linear impedance increase with frequency, due to the presence of multiple FSDs (DCSS1).

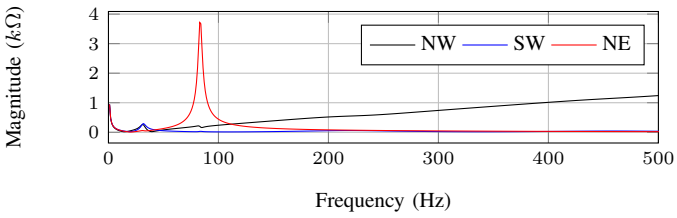

Fig. 9. DC grid frequency scan

B. Dynamic Performance with Generic Models

Fig. 10 shows the DC power (left) and voltage (right) for the GGG configuration following a coordinated reference step transitioning the system from N1a to N5a. The system exhibits a settling time of approximately 100 ms with well-damped oscillations at the DC grid resonance frequencies. Slight adaptations in power schedules occur due to the reduction in losses associated with the increased voltage profile.

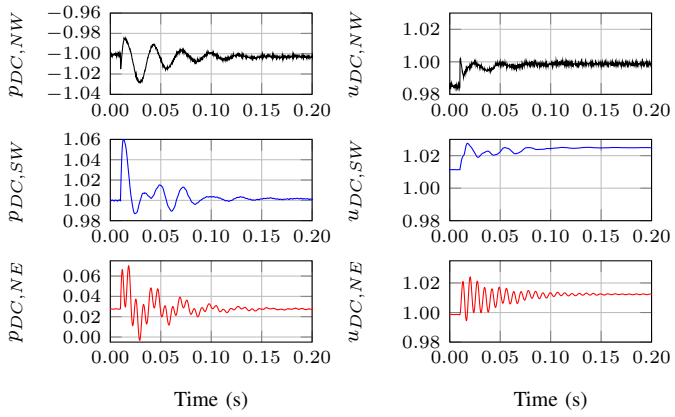

Fig. 10. Dynamic response for a change in OCs: from N1a to N5a

C. Contingency Analysis: Converter Blocking

Fig. 11 shows the DC power (left) and voltage (right) following the blocking of the negative pole at the NW station, which was initially exporting 1 GW to the AC grid. As a result, the DC voltage rises. In line with the LF results, the SW and NE stations share the power unbalance. Additionally, the DC voltage at the affected negative pole in the surviving stations temporarily exceeds the continuous operating range, reaching 547 kV (1.094 pu) at the NE station and 539 kV (1.078 pu) at the SW station. Minor disturbances occur on the healthy pole, but the DC voltage remains within the OSL. The behavior of the DC voltage at the blocked terminal is not critical for defining dynamic operating ranges and should be further examined within the scope of transient studies.

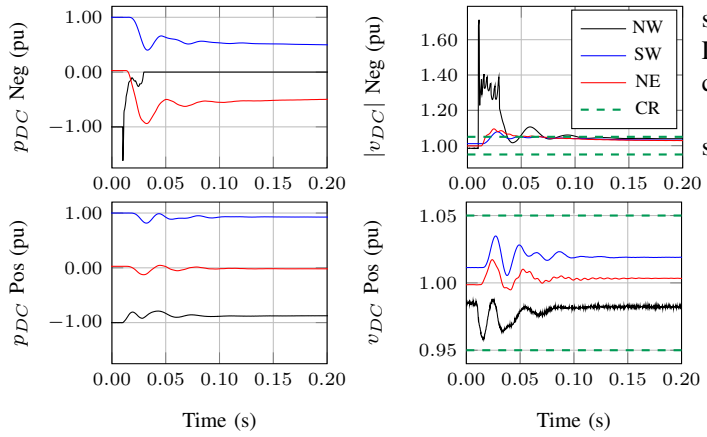

Fig. 11. Dynamic response for the NW-negative pole block

D. GGG configuration: Verification of Final States

Fig. 12 shows that for both configurations, GGG (top) and GGW (bottom), all scenarios remain within the OSL at the end of the primary DC voltage control action. Specifically:

- Red circles represent the initial OCs (N situations)
- For single pole outages (negative):
  - Green stars mark affected poles (surviving stations)
  - Blue start indicates healthy (positive) poles
- For bipolar outages, there are only blocked and surviving converters (no healthy pole)
- Pink circles show the blocked pole.

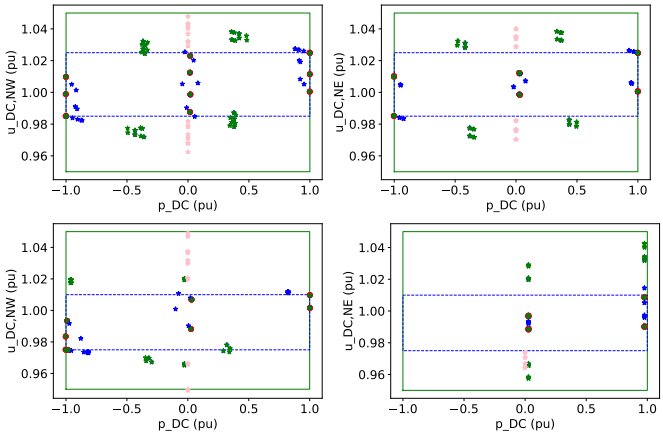

Fig. 12. Contingency analysis. GGG (top), GGW (bottom), NW (left), NE (right)

The operating points of the surviving terminals on both the affected and healthy poles shift according to the droop characteristics, with increased sensitivity as the DC voltage moves out of the secure range due to the LDCVSM settings. As previously mentioned, the blocked terminal may exhibit the highest pole-to-neutral voltage due to the neutral voltage shift caused by the asymmetrical operation.

VI. Conclusions

This work presents a scenario-based method for validating MT HVDC grid ratings, defining operating ranges, and setting primary DC voltage control parameters using DC LF calculations, focusing on N-1 rule compliance through contingency analysis.

Two configurations, differentiated by the connected AC system, are evaluated. It has been concluded that:

- Designing a 3T interconnector (GGG case) is relatively straightforward, as long as LDCVSM is available. In this setup, all stations share the responsibility for managing imbalances, and reserve capacity is naturally available.
- Incorporating a OWF introduces significant design constraints due the exclusion of the offshore station from the DC voltage control scheme and the resulting unavoidable DC voltage excursions associated with droop-type controls.

In the GGW configuration, the DC voltage at the offshore station inevitably rises after disturbances at the receiving end,

necessitating the allocation of significant security margins. This leads to upper voltage bounds that restrict operation to relatively low voltages, adversely impacting the system's economic performance due to increased losses. Operational constraints in the GGW configuration are particularly tight, with the secure range barely sufficient to accommodate DC grid voltage drops during maximum power exchanges. These challenges are expected to be mitigated in larger HVDC grids, where additional terminals assist with DC voltage regulation.

The study also highlights the impact of neutral voltage shifts during asymmetrical operation on the difference between pole-to-neutral and pole-to-ground voltages. In the test system, this gap can reach up to 1% of the nominal voltage, translating to 20% of the available continuous operating range, further constraining the design space if both quantities must remain within the OSL at all times.

If the proposed design proves impractical, allowing secondary control actions to restore DC voltage within the OSL and/or incorporating emergency OWF curtailment into the primary DC voltage control strategy could be a viable alternative. This would, however, require revisiting the design criteria that prohibit OSL violations after primary DC voltage control responses and considering other subsystem capabilities and has, therefore, being excluded from the InterOPERA project. Future work will focus on transient studies, including DC fault handling, with iteration on dynamic performance investigations to refine design and operational strategies.

VII. Appendix

A. Model Description

AC/DC converter are represented using the Generic MMC model available in EMTP® [18]. The bipole consists of two identical MMCs, each represented by an independent average arm model (model#3 in [19]). The negative terminal of the positive pole (and the positive terminal of the negative pole) is connected to the DMR. Each terminal is controlled by an independent module.

The generic control module is structured into upper and lower-level layers. The Lower Level Control module is encapsulated within a Dynamic Link Library (DLL) block and includes the Nearest Level Control (NLC) modulation. Since SMs are aggregated in the selected valve model, the Capacitor Balancing Algorithm (CBA) is not represented. The Upper Level Control generates the modulation index based on a classical vector control approach, allowing for an independent tracking of active power (or DC voltage) and reactive power (or AC voltage) references via a fast current control in the dq-frame. The control inputs the DC pole-to-neutral voltage by subtracting the DMR voltage from the measured pole-to-ground DC voltage [20]. An energy control has been added [21]. All measurements are low-pass filtered at 2 kHz.

Cables are represented using wideband models based on [17]. On the onshore AC side, a 400/280 kV transformer with a Ygd connection is considered, while on the DC side, a 150 mH inductance is added. For offshore station, two 66/280 kV transformer per pole are considered.

VIII. Acknowledgment

The authors gratefully acknowledge the contributions of participants in the InterOPERA HVDC grid design study task, particularly N. Krajisnik, B. Rennings, and F. Hassan for their valuable insights and engaging discussions.

References

[1] J. Liang, T. Jing, O. Gomis-Bellmunt, J. Ekanayake, and N. Jenkins, "Operation and control of multiterminal hvdc transmission for offshore wind farms," *IEEE Transactions on Power Delivery*, vol. 26, no. 4, pp. 2596–2604, 2011.

[2] J. Beerten, S. Cole, and R. Belmans, "Modeling of multi-terminal vsc hvdc systems with distributed dc voltage control," *IEEE Transactions on Power Systems*, vol. 29, no. 1, pp. 34–42, 2014.

[3] W. Wang and M. Barnes, "Power flow algorithms for multi-terminal vsc-hvdc with droop control," *IEEE Transactions on Power Systems*, vol. 29, no. 4, pp. 1721–1730, 2014.

[4] G. O. Kalcon, G. P. Adam, O. Anaya-Lara, S. Lo, and K. Uhlen, "Small-signal stability analysis of multi-terminal vsc-based dc transmission systems," *IEEE Transactions on Power Systems*, vol. 27, no. 4, pp. 1818–1830, 2012.

[5] J. Descloux, P. Rault, S. Nguefeu, J.-B. Curis, X. Guillaud, F. Colas, and B. Raison, "Hvdc meshed grid: Control and protection of a multi-terminal hvdc system," *CIGRE 2012*, pp. 1–10, 2012.

[6] L. Zhang, Y. Zou, J. Yu, J. Qin, V. Vittal, G. G. Karady, D. Shi, and Z. Wang, "Modeling, control, and protection of modular multilevel converter-based multi-terminal hvdc systems: A review," *CSEE Journal of Power and Energy Systems*, vol. 3, no. 4, pp. 340–352, 2017.

[7] E. Kontos, R. T. Pinto, S. Rodrigues, and P. Bauer, "Impact of hvdc transmission system topology on multiterminal dc network faults," *IEEE Transactions on Power Delivery*, vol. 30, no. 2, pp. 844–852, 2015.

[8] F. G. Puricelli, P. Rault, C. Cardozo, and J. Beerten, "Determination of sub-synchronous interactions between ac systems and grid-forming converters in bipolar hvdc connections," *IET Generation, Transmission & Distribution*, vol. n/a, no. n/a, pp. 1–17, 2024.

[9] M. Elsodany, K. Shinoda, J. Dai, A. Bertinato, and S. Bacha, "Assessment of two dc voltage droop options for small-signal stability in mmc-based multi-terminal dc grids," *IET Conference Proceedings*, vol. 2024, pp. 497–504, 2024.

[10] InterOPERA, "D2.1 functional requirements for hvdc grid systems and subsystems," tech. rep., June 2024.

[11] InterOPERA, "D1.1 requirements for ac/dc converter stations, dc switching stations, power park modules and dc grid controller offline models, sil models and c&p cubicles," tech. rep., September 2024.

[12] InterOPERA, "D4.2 multi-party cooperation framework – preliminary draft with focus on information sharing," tech. rep., December 2023.

[13] L. Papangelis, M.-S. Debry, P. Panciatici, and T. Van Cutsem, "Coordinated supervisory control of multi-terminal hvdc grids: A model predictive control approach," *IEEE Transactions on Power Systems*, vol. 32, no. 6, pp. 4673–4683, 2017.

[14] IEC, "Ts 63291-1:2023 - hvdc grid systems and connected converter stations - guideline and parameter lists for functional specifications - part 1: Guideline," 2023.

[15] Commission Regulation (EU), "2017/1485 of 2 august 2017 establishing a guideline on electricity transmission system operation," 2017.

[16] A. Allabadi, J. Mahseredjian, S. Dennetière, I. Kocar, and T. Ould-Bachir, "Integrating a novel hybrid ac-dc load-flow algorithm in an emt software," *CIGRE 2025 International Symposium*, 2025.

[17] T. Karmokar and M. Popov, "Enhanced modelling and parameter determination of hvdc cables using practice-oriented methodology," *CIGRE CSE 036*, 2025.

[18] H. Saad, J. Mahseredjian, and S. Dennetière, "Modular multilevel converter in emtp-rv," tech. rep., 2014.

[19] H. Saad, S. Dennetière, J. Mahseredjian, P. Delarue, X. Guillaud, J. Peralta, and S. Nguefeu, "Modular multilevel converter models for electromagnetic transients," *IEEE Transactions on Power Delivery*, vol. 29, no. 3, pp. 1481–1489, 2014.

[20] CIGRE, "Tb 604 guide for the development of models for hvdc converters in a hvdc grid," 2014.

[21] J. Freytes, G. Bergna, J. A. Suul, S. D'Arco, F. Gruson, F. Colas, H. Saad, and X. Guillaud, "Improving small-signal stability of an mmc with ccsc by control of the internally stored energy," *IEEE Transactions on Power Delivery*, vol. 33, no. 1, pp. 429–439, 2018.